Electronic Supplementary Material (ESI) for Chemical Communications.
This journal is © The Royal Society of Chemistry 2023

Supporting Information

Defect passivation via a multifunctional organic additive toward efficient and stable inverted perovskite solar cells

Chufeng Qiu[a,b], Jiaxing Song[*a], Yan Wu[a], Xinxing Yin[a], Lin Hu[a], Zhen Su[a], Yingzhi Jin[a], Wentao Wang[*b], Hao Wang[a], Zaifang Li[*a]

[a] China-Australia Institute for Advanced Materials and Manufacturing, Jiaxing University, Jiaxing 314001, PR China

[b] School of Materials Science and Engineering, Zhejiang Sci-Tech University, Hangzhou 310018, PR China

Experimental

Materials

Chlorobenzene (CB, 99.8%), N, N-Dimethylformamide (DMF, 99.8%), and Dimethyl sulfoxide (DMSO, 99.7%) were purchased from Sigma-Aldrich. Methyl 3-amino-2-thiophenecarboxylate (MATC, 99%) was purchased from Energy Chemical. Formamidine Hydroiodide (FAI, ≥99.5%), Cesium iodide (CsI, 99.9%), Lead iodide (PbI_2, >99.99%), Lead bromide ($PbBr_2$, >99.99%), Fullerene-C60 (C60, >99%), 2,9-dimethyl-4,7-diphenyl-1,10-phenanthroline (BCP, >99%), and Poly[bis(4-phenyl) (2,4,6-triMethylphenyl)aMine] (PTAA) were purchased from Xi'an Polymer Light Technology Corp. Poly [(9,9-bis(3'-(N,Ndimethyl)-NethylaMMoiniuM-propyl)-2,7-fluorene) -alt-2,7-(9,9-dioctylfluorene)]dibroMide (PFN-Br) were obtained from Luminescence Technology Corp. All chemicals and reagents were used without further purification.

Device Fabrication

First of all, all etched ITO conductive glasses were cleaned with deionized water, acetone, and isopropanol in sequence by 30 min ultrasonication. After washing, the substrates were dried with a nitrogen gas flow. Before spin-coating, the ITO substrate was treated with plasma for 6 minutes, and then transferred to the glove box. The PTAA was dissolved in toluene to prepare a solution of 2 mg/ml, and the solution was spin-coated on the ITO surface at a rate of 6000 rpm for 30 s, follow by annealing at 100 °C for 10 min. After the substrate cooling down to room temperature, 0.5 mg/mL of PFN-Br dissolved in DMF was spin-coated on the surface of PTAA at 5000 rpm for 20 s. The mixed perovskite precursor solution was prepared by dissolving FAI (171.3 mg), CsI (53.0 mg), PbI_2 (493.7 mg), and $PbBr_2$ (66.0 mg) in 1mL mixed solution of DMF and DMSO (volume ration of DMF/DMSO is 4:1). The perovskite precursor solution was spin-coated on the substrates by a consecutive two-step spin-coating process at 1000 rpm for 10 s and at 6000 rpm for 30 s, respectively. During the second step, 150 μL of CB antisolvent containing MATC was dropped on the substrate at 15 s before the end. The wet film were immediately annealed at 100 °C for 10 minutes. Then, 20 nm C60 and 5 nm BCP were sequentially deposited on the surface of perovskite by thermal evaporation. Finally, 80 nm Ag electrode was vacuum thermally deposited through a shadow mask.

Film characterization

Density functional theory (DFT), as implemented in Vienna *ab* initio simulation package (VASP), was used to carry out the calculations presented here. The projector augmented wave (PAW) method was used to treat the effective interaction of the core electrons and nucleus with the valence electrons, while exchange and correlation were described using the generalized gradient approximation (GGA) of the Perdew-Burke-Ernzerhof (PBE) functional. The cut-off energy is set at 400 eV for the plane-wave basis restriction in the calculations. K-points are sampled under the Monkhorst-Pack scheme for the Brillouin-zone integration (K-points were sampled using 3×3×1 mesh). In all calculations, the forces acting on all atoms are less than 0.02 eV/Å in fully relaxed structures, and self-consistency accuracy of 10^{-5} eV is reached for electronic loops.

The X-ray diffraction (XRD) patterns were obtained by the Rigaku Ultima IV instrument using

Cu Kα radiation with a rated output of 3 Kw. UV-vis absorption spectra were obtained from a USA Perkin Emmer (PE) Lambda 365 UV spectrometer. The water contact angle was obtained by the contact angle measuring instrument (TBU100). The top-viewed SEM images were obtained by Zeiss Sigma 300 Schottky field emission electron microscopy measurements. Fourier transform infrared spectroscopy (FTIR) spectra were obtained from Shimadzu IRTracer-100 measurements. X-ray photoelectron spectroscopy (XPS) data were collected with a Thermo Scientific K-Alpha+ system. The samples were measured using an Al K Alpha source. The core level spectra were recorded using a pass energy of 50 eV from an analysis area of 400 μm×400 μm. Steady-state photoluminescence (PL) and time-resolved photoluminescence (TRPL) spectra were obtained by FLS 1000 photoluminescence spectrometer in Edinburgh. An excitation source wavelength of 510 nm was used for PL measurements.

Device characterization

The current density-voltage (*J-V*) characteristics of devices were measured in glove-box under 100 mW/cm^2 AM 1.5G solar irradiation (Enlitech SS-F5-3A) with a Keithley 2400 Source Meter. The *J-V* curves of all devices were characterized using a metal mask with an active area of 0.0975 cm^2 and measured by reverse scans (1.5 V to -0.5 V bias). The external quantum efficiency (EQE) spectra were taken on a QE-R3011 system (Enli Tech). The dependence of J_{sc} on P_{light} can provide information on the bimolecular recombination occurring in the photoactive layer, which follows a power law dependence, that is, $J_{sc} \propto P_{light}^{\alpha}$. The V_{oc} varies logarithmically with P_{light} and follows the relationships of $V_{oc} \propto (nkT/q)\ln(P_{light})$. The electrochemical impedance spectroscopy (EIS) was measured in a frequency range from 0.1 Hz to 100 MHz by Shanghai Chenhua CHI608E electrochemical workstation. Space charge limited current (SCLC) was conducted by testing the electron-only device with the structure of ITO/SnO_2/perovskite/C_{60}/BCP/Al, and testing the hole-only device with the structure of ITO/PTAA/perovskite/Au.

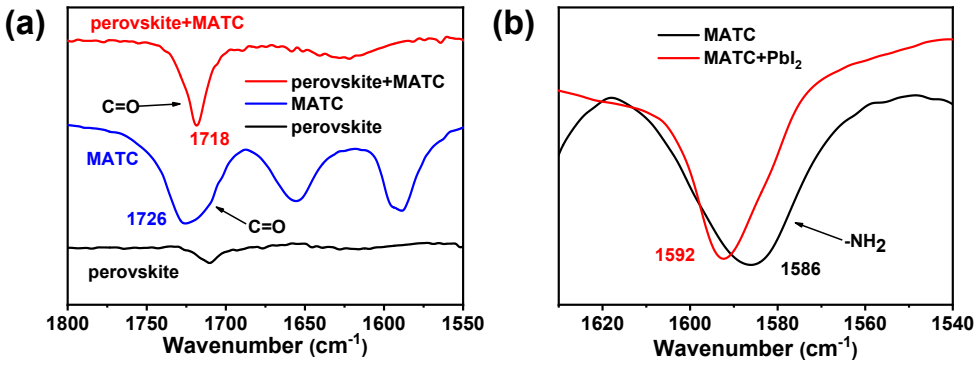

Figure S1. FTIR characterization of the interaction between MATC and Pb^{2+} in the perovskite.

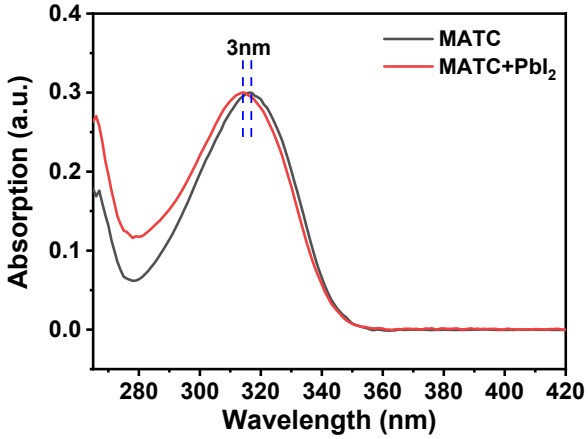

Figure S2. UV-vis absorption spectra of MATC and MATC/PbI_2 solution.

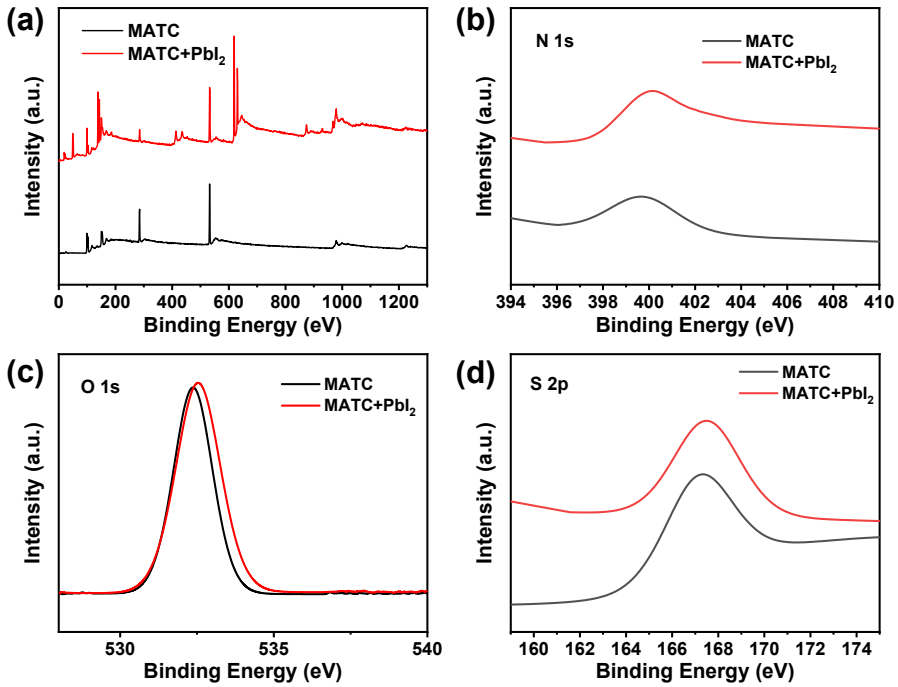

Figure S3. Characterization of the interaction between MATC and perovskite. XPS patterns of (b) N 1s, (c) O 1s and (d) S 2p for MATC with and without PbI_2.

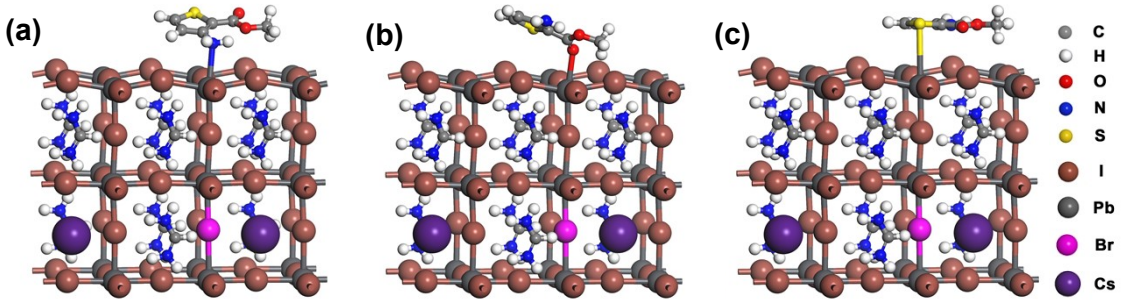

Figure S4. Theoretical models of perovskite with molecular interaction of Pb^{2+} with MATC: (a) $–NH_2$, (b) C=O, (c) thiophene.

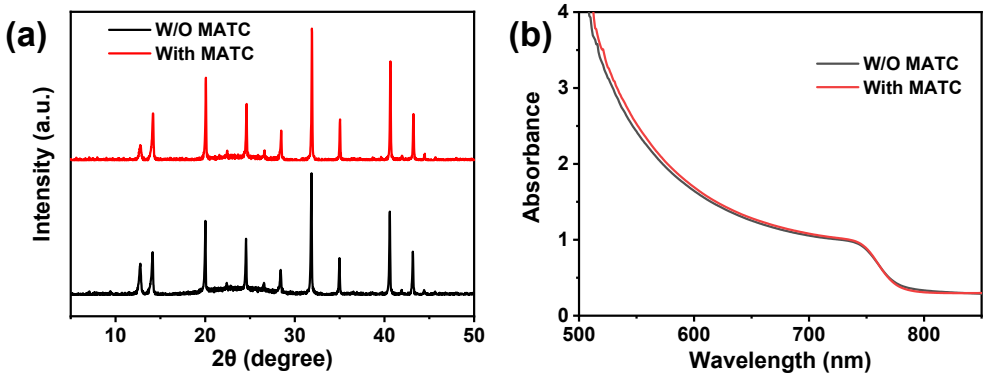

Figure S5. (a) XRD patterns and (b) UV-vis absorption spectra of perovskite films with and without MATC.

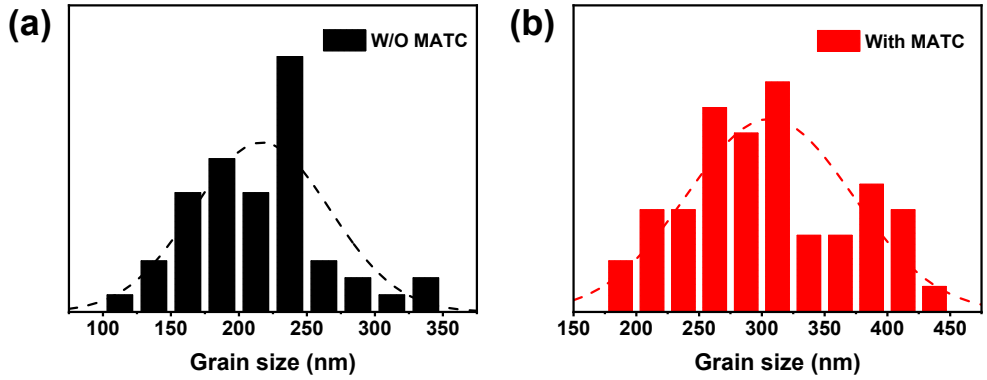

Figure S6. Grain size statistics of perovskite films with and without MATC.

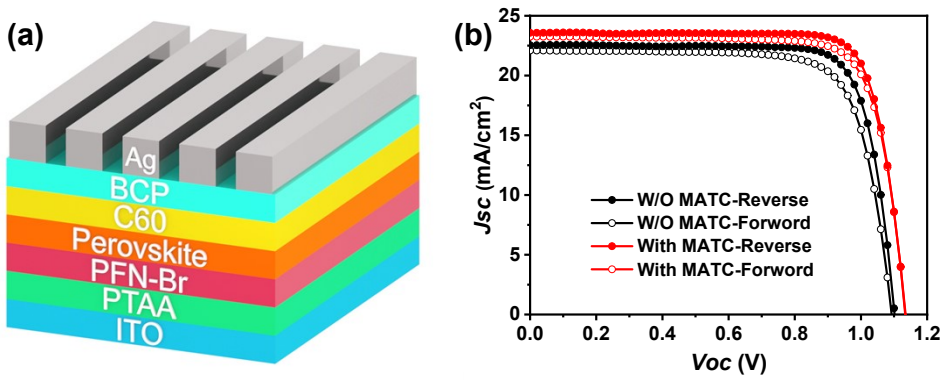

Figure S7. (a) Schematic diagram of the device structure. (b) Reverse and forward *J-V*

characteristics of PSCs with and without MATC.

Table S1. The average photovoltaic parameters of PSCs with various concentrations of MATC obtained based on 20 cells. Parameters of the best cell are reported in brackets.

MATC	V_{oc} (V)	J_{sc} (mA/cm^2)	FF (%)	PCE (%)
0 mg ml^{-1}	1.091±0.01 (1.102)	22.06 ± 0.5 (22.52)	77.96 ± 0.9 (79.28)	18.76 ± 0.6 (19.67)
2.0 mg ml^{-1}	1.110 ± 0.01 (1.114)	22.44 ± 0.3 (22.86)	79.69 ± 0.6 (80.11)	19.84 ± 0.4 (20.41)
3.5 mg ml^{-1}	1.122 ± 0.01 (1.135)	22.93 ± 0.3 (23.57)	79.93 ± 0.4 (80.39)	20.56 ± 0.5 (21.51)
5.0 mg ml^{-1}	1.110 ± 0.01 (1.124)	21.49 ± 0.5 (22.00)	79.56 ± 0.5 (80.12)	18.98 ± 0.6 (19.81)

Table S2. Photovoltaic parameters of PSC devices with and without MATC obtained from Figure S7.

		V_{oc} (V)	J_{sc} (mA/cm^2)	FF (%)	PCE (%)	HI (%)
W/O	Reverse	1.102	22.52	79.28	19.67	7.0
	Forword	1.092	22.09	75.88	18.30	

With	Reverse	1.135	23.57	80.39	21.51	3.9
	Forword	1.133	23.25	78.42	20.66	

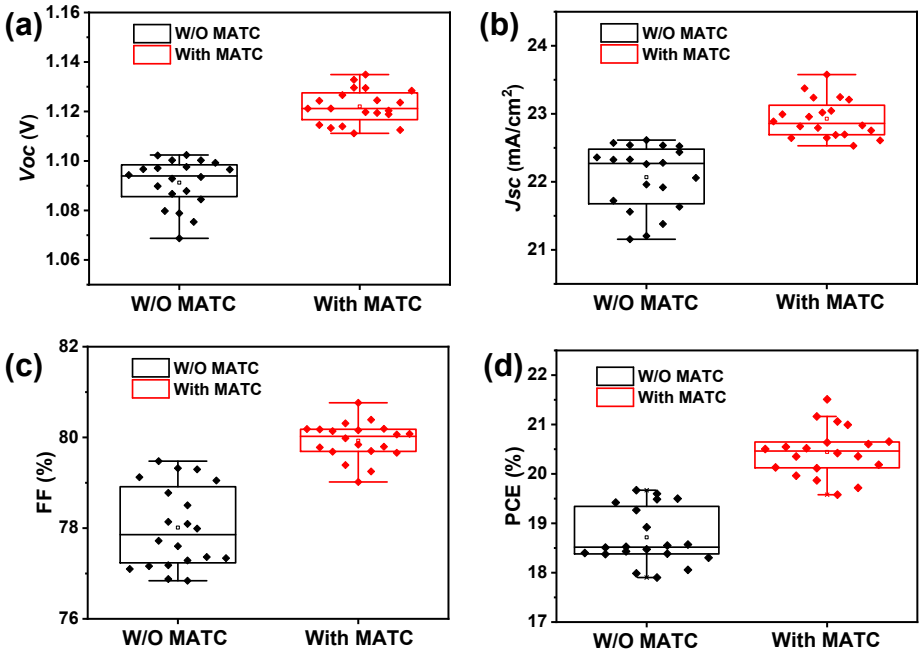

Figure S8. Statistics of photovoltaic parameters (V_{oc}, J_{sc}, FF, and PCE) for the PSC devices with and without MATC.

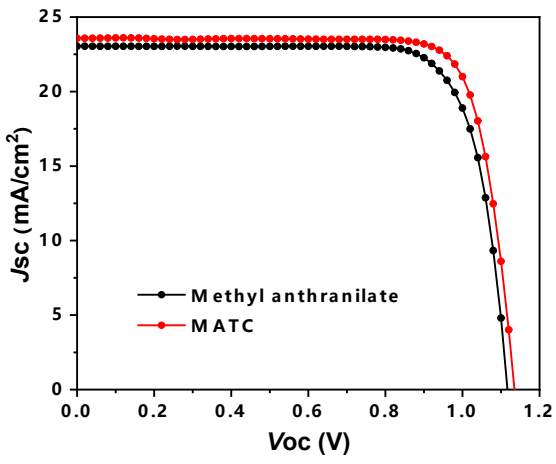

Figure S9. The *J-V* characteristics of the best PSCs with the addition of optimized MATC and methyl anthranilate. The optimal concentration of MATC and methyl anthranilate was 3.5 and 2.0 mg/ml, respectively.

Table S3. Photovoltaic parameters of the best PSCs with the addition of MATC and methyl anthranilate. The average values are obtained based on 20 cells and reported in brackets.

Additive	V_{oc} (V)	J_{sc} (mA/cm^2)	FF (%)	PCE (%)
MATC	1.135	23.57	80.39	21.51
	(1.122±0.01)	(22.93±0.3)	(79.93±0.4)	(20.56±0.5)
Methyl anthranilate	1.120	23.04	80.16	20.68
	(1.112±0.01)	(22.21±0.7)	(79.52±0.6)	(19.64±0.7)

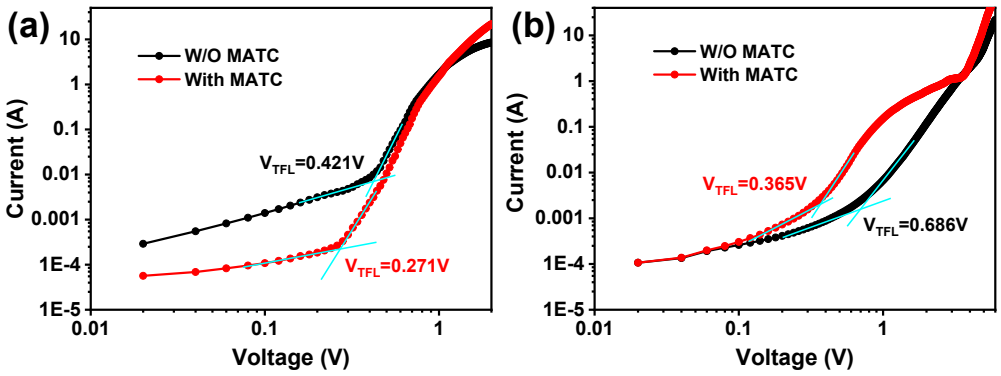

Figure S10. *J-V* curves of (a) hole-only and (b) electron-only devices with and without MATC.

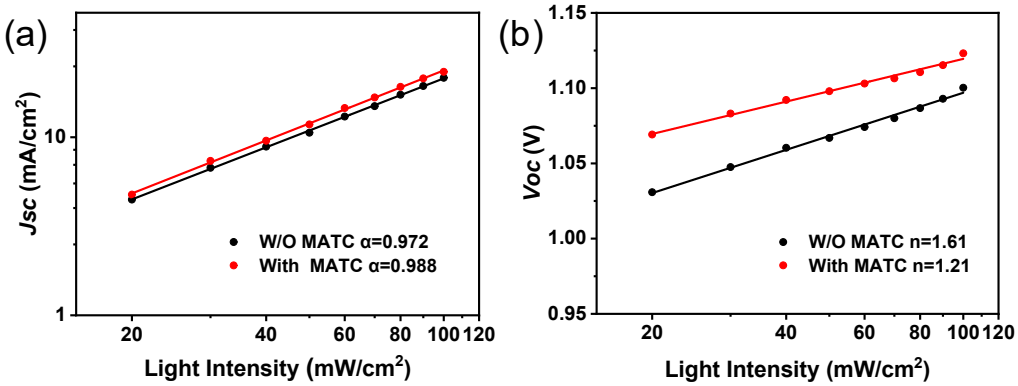

Figure S11. (a) J_{sc} and (b) V_{oc} dependence on the light intensity for the devices with and without MATC.

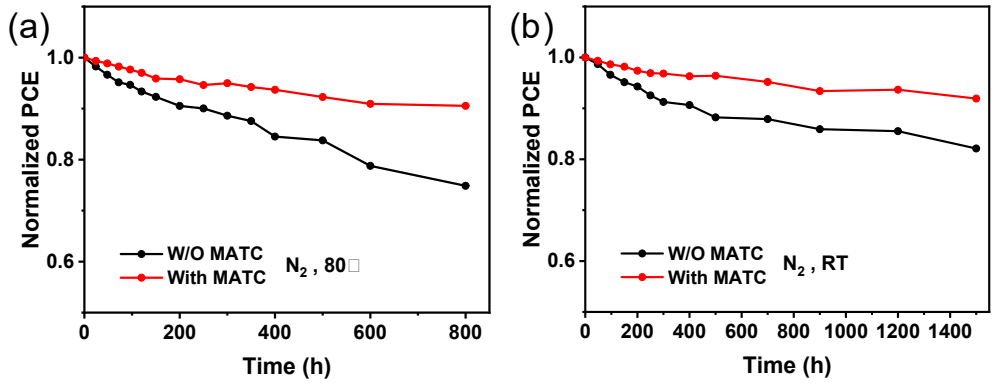

Figure S12. Normalized PCE of the unencapsulated device as a function of (a) heat time in glovebox at 80 °C, and (b) storage time in glovebox at room temperature.